NASA TM X- 70533

QUANTITATIVE MAGNETOSPHERIC MODELS DERIVED FROM SPACECRAFT MAGNETOMETER DATA

GILBERT D. MEAD

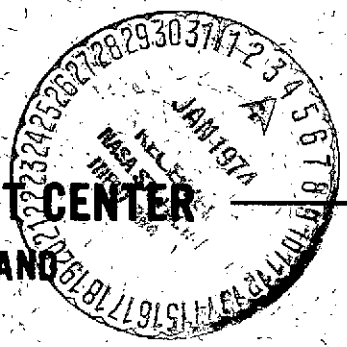DONALD H. FAIRFIELD

NOVEMBER 1973

GSFC —— GODDARD SPACE FLIGHT CENTER ——
GREENBELT, MARYLAND

j

QUANTITATIVE MAGNETOSPHERIC MODELS DERIVED

FROM SPACECRAFT MAGNETOMETER DATA

Gilbert D. Mead

Laboratory for Space Physics

and

Donald H. Fairfield

Laboratory for Extraterrestrial Physics

NASA Goddard Space Flight Center

Greenbelt, Maryland 20771

November 1973

ABSTRACT

Quantitative models of the external magnetospheric field have been derived by making least-squares fits to magnetic field measurements from four IMP satellites. The data set consists of 12,616 vector field averages over half-R_E intervals between 4 and 17 R_E, taken from 451 satellite orbits between 1966 and 1972. The data were fit to a power series expansion in the solar magnetic coordinates and the solar wind-dipole tilt angle, and thus the models contain the effects of seasonal north-south asymmetries. The expansions are divergence-free, but unlike the usual scalar potential expansions, the models contain a non-zero curl representing currents distributed within the magnetosphere. Characteristics of four models are presented, representing different degrees of magnetic disturbance as determined by the range of Kp values. The latitude at the earth separating open polar cap field lines from field lines closing on the dayside is about 5° lower than that determined by previous theoretically-derived models. At times of high Kp, additional high-latitude field lines are drawn back into the tail. Near solstice, the separation latitude can be as low as 75° in the winter hemisphere. The average northward component of the external field is much smaller than that predicted by theoretical models, indicating the important effects of distributed currents in the magnetosphere. Current densities implied by the models are of the order of 10^{-9} amp/m^2 across the magnetotail.

INTRODUCTION

Quantitative models of the geomagnetic field generally fall into two types: those that describe the field due to sources inside the earth (internal models) and those which attempt to describe the effect of currents located above the earth's surface (external models). Internal models are derived from direct measurements of one or more components of the field. Since the time of Gauss, spherical harmonic expansions of a scalar potential have been used to fit these measurements. Similar techniques have been used to model the overhead current systems responsible for the diurnal and lunar variations in the surface field. However, up until now quantitative models of the external magnetospheric field have not been based on field measurements or are based only indirectly on them. Some of these models (Mead, 1964; Midgley, 1964; Olson, private communication; Choe and Beard, 1973) have been based on theoretical solutions to the traditional Chapman-Ferraro problem of an unmagnetized plasma incident upon a magnetic dipole (e.g., Mead and Beard, 1964; Olson, 1969; Choe et al., 1973). In these models the resulting external field is expressed in terms of a scalar potential, expanded in spherical harmonics and modified to reflect the fact that the current sources are external to the region of the expansion. Others (Hones, 1963; Taylor and Hones, 1965; Williams and Mead, 1965; Antonova and Shabanskiy, 1968; Sugiura and Poros, 1973; Olson and Pfitzer, 1973) have been based partly on theory and partly on known characteristics of the external field. These models have used some combination of spherical harmonics, image dipoles and/or current sheets to describe the magnetospheric field. The characteristics of many of these models have been discussed by Roederer (1969).

In this study we have made two major departures from previous work. First of all, we follow procedures heretofore used only in modelling the internal field, namely, making least-squares fits to a body of magnetometer data using a model with adjustable coefficients. The data set consists of magnetometer measurements from four spacecraft: Explorer 33 (A-Imp-D), Explorer 34 (Imp 4), Explorer 41 (Imp 5), and Explorer 43 (Imp 6). These spacecraft were in highly eccentric orbits, with apogee ranging from 29 to 80 R_E. The data were obtained over an interval of almost six years on 451 separate spacecraft orbits.

Secondly, we found it necessary to abandon the use of a scalar potential with its implicit assumption that there are no current sources in the region of the expansion. Instead, we used power series expansions of the field components themselves in the solar magnetic coordinates and the tilt angle. Although $\nabla \times \vec{B} \neq 0$ in our expansions, indicating the presence of distributed currents, the fitting program constrained the coefficients so as to make $\nabla \cdot \vec{B} = 0$.

The coefficients and characteristics of four models are presented in this study. These models contain terms up to quadratic in the solar magnetic coordinates and linear in tilt angle. Each was derived by least-squares fits to subsets of the data sorted according to the Kp value. The models contain only terms which retain the obvious east-west and summer-winter symmetries.

By taking the curl of the resulting expressions for the magnetic field, a general picture of the currents can be determined. Although the models do not contain sufficiently high-order terms to determine these currents with much precision, current densities of the order of 10^{-9} amp/m^2 in the outer magnetosphere are implied by the models.

Since the models are derived from measurements of the external field, the accuracy of the models is limited by the spatial coverage of the data. No data was used beyond 17 R_E, and therefore the models should not be used to calculate magnetic fields beyond this distance. Very little data was available inside 5 R_E, and therefore the models do not accurately represent the field depressions observed by Sugiura (1973) and others at 2-5 R_E. In addition, data were often not available at some longitudes during certain seasons. These gaps in the data coverage, together with the constant variability in magnetospheric configuration, limited us to very simple models.

In this paper a number of model characteristics are compared with experimental results previously presented by Fairfield (1968, 1971), Sugiura et al. (1971), Sugiura (1972a), and Skillman (1973). In a companion paper (Fairfield and Mead, 1973) the models are used to map field lines between low altitudes and the distant magnetosphere so as to compare, for example, the observed positions of the high-latitude boundary of the trapping region with the polar cap field lines as determined by the various models.

TREATMENT OF DATA

The magnetic field data used as the starting point in this study were averages of the three vector components over telemetry sequences of duration 81 sec (Explorer 33), 20.5 sec (Explorers 34 and 41), and 15.4 sec (Explorer 43). These experiments have been described previously (Behannon, 1968; Fairfield, 1969; Fairfield and Ness, 1972; Fairfield, 1973a); all were performed on magnetically clean spacecraft, yielding vector field measurements with an absolute accuracy of better than 1 gamma. The least sensitive ranges of the four instruments, which determined the earthward termination of the data, were $\pm64\gamma$ (Explorer 33), $\pm128\gamma$ (Exlorer 34), $\pm200\gamma$ (Explorer 41), and $\pm432\gamma$ (Explorer 43). Thus no measurements were available inside 4 R_E, and relatively few inside 5 R_E.

Plots of both the measured sequence averages and the theoretical predictions from a model of the internal field were used to identify magnetopause crossings and to detect and eliminate measurements which were contaminated by telemetry noise. (For examples of these plots see Fairfield and Ness, 1972; Fairfield, 1973b.) Data taken outside the magnetopause were eliminated for the present analysis.

Since both time and spatial variations were small between sequence averaging intervals, further averaging was clearly desirable in order to minimize redundant data and reduce the data set to a manageable size. In order to minimize the effect of variations in the internal field over the averaging interval, the quantities ΔB, ΔI, and ΔD were calculated for each telemetry sequence, where ΔB is the difference in magnitude between

the measured and internal reference field, and ΔI and ΔD are the inclination and declination differences (Mead and Cahill, 1967). The internal reference field was, in most cases, the IGRF model (IAGA, 1969). These differences were then averaged over half-earth-radii intervals of radial distance. Typical averages were over 10 to 15 minutes of time, thus suppressing the most rapid time variations. (The orbit of Explorer 33 was more circular than the others, and there we also required that the averaging interval not exceed 5° in longitude.) Associated with each of these data points was the average spacecraft position in solar magnetic coordinates, the tilt angle T, and the time of the measurement. Only data within 17 R_E was included in this analysis, as we felt that our simple model expansions would have difficulty in simultaneously fitting the near-earth data and the distant tail field data.

The extent of the data set is described in Table 1. The data were obtained over an interval of almost six years, covering 4340 spacecraft hours within the magnetosphere on 451 separate spacecraft orbits. Over 4×10^7 individual vector measurements were combined into 12,616 half-earth-radii averages.

The data were then separated into two roughly equal parts, depending on the Kp value at the time each measurement was made. The quiet data included measurements for which Kp < 2; for the disturbed data, Kp $\geq$ 2. Subsequently, two more limited subsets were created, a super-quiet (Kp = 0, 0^+ data set and a super-disturbed (Kp $\geq$ 3) set.

To prevent regions with a high concentration of data from having a disproportionately large effect on the models, we decided to carry out further averages over our four-dimensional space. Intervals of solar magnetic latitude and longitude were chosen so as to divide a sphere around the earth into 96 equal solid angles (see Fairfield and Ness, 1967, for definition of the angles). This division, together with 13 radial intervals of 1 R_E (4 < R < 17 R_E) and 7 tilt-angle intervals of 10° (-35° < T < 35°) defined 96 × 13 × 7 = 8736 four-dimensional "buckets". Each data point was then sorted into the appropriate bucket and the spatial parameters and field values within a given bucket were averaged. Four final data sets resulted: the quiet-time data, with 2368 points; the disturbed data, with 2206 points; the super-quiet data, with 882 points; and the super-disturbed data, with 1334 points.

This data, however, was by no means uniformly distributed over our four-dimensional space. Each spacecraft traverses a limited range of latitudes and, furthermore, makes measurements within a given longitude sector only during certain times of the year, when the range of tilt angles is correspondingly limited. The resulting non-uniform distribution of data can only be minimized by having a large number of spacecraft with a variety of orbital configurations.

If the quiet data had been evenly distributed, about 85% of the buckets inside the magnetopause would have contained a single point. In fact, however, only 31% of these buckets were filled, with a maximum of 12 points and an average density of 2.7 points per bucket. The empty buckets are at latitudes not sampled by the various spacecraft and at certain longitudes not sampled for certain tilt angles.

The distribution of data is illustrated in Figure 1, which indicates the magnetic latitude and local time of each point in the final data set (quiet and disturbed combined) for distances of 6-8 R_E (top) and 13-15 R_E (bottom). The near-earth data indicates a scarcity of points near the magnetic equatorial plane and better latitudinal coverage in the northern hemisphere compared to the southern hemisphere. There are practically no measurements south of -50° latitude. At the greater distances, data is absent near the noon meridian because such measurements would be outside the magnetopause. Fewer high-latitude data are present at greater distances, because the spacecraft are closer to apogee, which for all spacecraft is in the vicinity of the solar ecliptic equatorial plane.

The various symbols indicate tilt angles within three different ranges. It is clear that coverage in certain latitude-local time regions is restricted to certain seasons. Particularly apparent in the near-earth distribution is a lack of southern hemisphere data in the nightside hemisphere for positive tilt angles and in the dayside hemisphere for negative tilt angles. These gaps in the four-dimensional data distribution mean that a least-squares model will be poorly constrained in regions where there is no data. This situation imposes a severe limitation on these models, a point which will be discussed further in a later section.

RESULTS

In the initial phase of the study we attempted to fit the measured difference field with spherical harmonic expansions of the scalar potential similar to those used by Mead (1964) in his theoretically-derived model of the external field. The values of the coefficients resulting from fits to different components, however, were very different from each other. We concluded that the assumption that the region was source-free was simply not valid; distributed currents within the region of measurements, which cannot be represented by a scalar potential, made a substantial contribution to the difference field.

Since Mead (1964) had noted that the expansion of the external field was particularly simple when expressed in cartesian coordinates, we transformed the difference field into cartesian coordinates (ΔB_x, ΔB_y, and ΔB_z) and modified our least-squares program so as to fit each component to a power series expansion in cartesian solar magnetic coordinates, including terms linear in the tilt angle. (In this coordinate system the z-axis is aligned with the magnetic dipole, the x-z plane contains the earth-sun line, positive values of x are on the dayside and the y-axis is in the dusk meridian. The tilt angle, T, is the complement of the angle between the z-axis and the earth-sun line, or, equivalently, the geomagnetic latitude of the subsolar point; it is positive during northern hemisphere summer.)

Neither $\nabla \cdot \vec{B}$ nor $\nabla \times \vec{B}$ necessarily vanished with this expansion. However, the coefficients obtained for a quadratic fit (20 coefficients

for each component, totaling 60) were found to come very close to satisfying the $\nabla \cdot \vec{B} = 0$ condition, although $\nabla \times \vec{B}$ was clearly non-zero. This low value of $\nabla \cdot \vec{B}$ gave us great confidence in the self-consistency of the underlying data (although since the data was not taken at one instant of time there was no reason to expect $\nabla \cdot \vec{B}$ to be identically zero).

Thus encouraged, we developed a more general least-squares program, using a method of Lagrangian multipliers, to fit all three components of the field simultaneously, <u>subject to the condition that the coefficients satisfy the $\nabla \cdot \vec{B} = 0$ requirement.</u> (For the quadratic fit, eight equations of constraint were imposed; thus there were only 52 independent coefficients.) The imposition of the $\nabla \cdot \vec{B} = 0$ condition changed the values of the largest coefficients by only a few percent and <u>the residuals increased by less than 1%</u> (see below for definition of the root-mean-square vector residual field).

Two 60-coefficient models resulting from this program have been made available to a number of workers and have been used as the basis for a few subsequent papers. In these models all possible terms through quadratic in the solar magnetic coordinates and linear in the tilt angle were included, with no symmetry imposed. The models, however, showed a high degree of both dawn-dusk and north-south symmetry. The dawn-dusk symmetry was greatest about a meridian plane rotated about 4° from the solar direction, an angle about equal to the aberration of the solar wind direction caused by the orbital motion of the earth. Also, the field-line topology in one hemisphere for a given positive tilt angle was very similar to the topology in the opposite hemisphere for the same negative tilt. It

was not possible, however, to determine whether the small dawn-dusk and north-south asymmetries represented real asymmetries in the magnetosphere, or whether they were caused by time variations and non-uniformities in the distribution of data. Since we had no assurance of the reality of the model asymmetries, we developed a modified least-squares program to fit an expansion containing only those terms which retained both types of symmetries. The dawn-dusk symmetry condition requires that

$$\Delta B_x(-Y) = \Delta B_x(Y) \tag{1}$$

$$\Delta B_y(-Y) = -\Delta B_y(Y) \tag{2}$$

$$\Delta B_z(-Y) = \Delta B_z(Y) \tag{3}$$

for all X, Y, Z, and T. North-south symmetry requires that

$$\Delta B_x(-T,-Z) = -\Delta B_x(T,Z) \tag{4}$$

$$\Delta B_y(-T,-Z) = -\Delta B_y(T,Z) \tag{5}$$

$$\Delta B_z(-T,-Z) = \Delta B_z(T,Z) \tag{6}$$

These conditions (which are automatically satisfied for a dipole field) eliminate almost three-fourths of the coefficients, and the quadratic expansion becomes

$$\Delta B_x = a_1 Z + a_2 XZ + T(a_3 + a_4 X + a_5 X^2 + a_6 Y^2 + a_7 Z^2) \tag{7}$$

$$\Delta B_y = b_1 YZ + T(b_2 Y + b_3 XY) \tag{8}$$

$$\Delta B_z = c_1 + c_2 X + c_3 X^2 + c_4 Y^2 + c_5 Z^2 + T(c_6 Z + c_7 XZ) \tag{9}$$

(note comments on units below), subject to the $\nabla \cdot \vec{B} = 0$ conditions:

$$a_2 + b_1 + 2c_5 = 0 \tag{10}$$

$$a_4 + b_2 + c_6 = 0 \tag{11}$$

$$2a_5 + b_3 + c_7 = 0 \tag{12}$$

This is a 17-coefficient expansion, with three restrictions, making 14 independent coefficients.

Since the preliminary work had indicated that the optimum plane of symmetry would be rotated a few degrees from the noon-midnight meridian, the X and Y coordinates and field components were rotated through an arbitrary angle before determining the least-squares coefficients to the symmetric expansion. Residuals were then calculated for various rotation angles. A minimum in the residuals was reached at a rotation angle of from 3 to 5 degrees, depending upon the data set, beyond which the residuals began to increase. For the more disturbed data sets, the rotation angle for minimum residuals was less than for the quiet data sets, suggesting that the aberration angle is less during disturbed times, when the average solar wind velocity is probably higher. Our results do _not_ support the suggestion made by Cummings et al. (1971), based on analysis of ATS-1 magnetometer data, that the plane of maximum symmetry is rotated by 10-15°. We found the residuals for such large rotation angles to be significantly larger than for angles of 3-5°.

The residuals for the 17-coefficient symmetric model with a rotation of 4° were only about 4% larger than the residuals for the 60-coefficient model with no symmetry imposed. The fact that elimination of over seventy percent of the coefficients only increased the residuals by this small amount gave us added confidence in the basic symmetry of the underlying data.

In addition to a quiet and a disturbed model, coefficients were also determined for a super-quiet and a super-disturbed model. The coefficients (in gammas) for all four of these models are listed in Table 2, valid for X, Y, and Z given in units of tens of earth radii (1 R_E = 6378 km) and T in units of tens of degrees. These units were chosen so as to make the

contribution from each term, in gammas, roughly proportional to the

magnitude of the corresponding coefficient for moderate tilt angles ($\simeq 10^{\circ}$)

at geocentric distances of about 10-15 R_E.

Perhaps the most obvious feature of the coefficients is the tendency

for them to increase in magnitude with increasing Kp, indicating generally

larger magnetospheric distortions during times of enhanced magnetic activity.

It is particularly interesting that the c_1 coefficient has a negative sign.

This term is equivalent to the $\bar{g}_1^0$ term in the Mead (1964) model, which gave

a northward field of 25γ for a sub-solar boundary distance r_b = 10 R_E.

The c_1 coefficient in these models, however, gives a southward field of

10-19γ, depending on the Kp range. Since currents at the magnetopause

give rise to a northward-directed field, this result implies that the

distributed currents within the magnetosphere give rise to a southward

field near the earth which more than offsets the effect of the magnetopause

currents. (The c_3 and c_4 terms increase the ΔB_z component in the outer

magnetosphere; thus the average measured value of ΔB_z was actually -1.6γ

for the quiet data and -5.5γ for the disturbed data.) The total field

magnitude in the equatorial plane near the earth calculated from these

models is much less than the average magnitude predicted by a model con-

taining boundary currents only. This is consistent with Sugiura's (1972a)

results indicating negative values of ΔB near the magnetic equatorial plane

close to the earth. It is clear that any realistic model of the magneto-

spheric field must have the ability to describe distributed currents.

The coefficient with the largest magnitude is a_1, which gives a

field directed generally towards the sun in the northern hemisphere and

away from the sun in the southern hemisphere, thus producing oppositely-directed fields on either side of the plasma sheet in the geomagnetic tail. Another large term is c_2, giving a northward field on the dayside and a southward field on the nightside. A restriction that the models be curl-free would have required $a_1 = c_2$, and these coefficients would then be the equivalent of $\sqrt{3} \; g_2^{-1} = 21\gamma/10 \; R_E$ in the <u>Mead</u> (1964) model. Thus, the values of a_1 and c_2 in the MF73Q model agree quite well with Mead's earlier value of g_2^{-1}, and the fact that $a_1 > c_2$ is an indication of a magnetospheric current directed from dawn to dusk (see discussion of curl $\vec{B}$ in a later section).

The root-mean-square values of the measured vector difference field, $|\Delta\vec{B}|_{rms}$, and the vector residual field $|\Delta\vec{B}|_{res}$ for each of these models is shown in <u>Table 3</u>. These quantities are defined by:

$$|\Delta\vec{B}|_{rms} = \left| \sum_{i=1}^{N} (\vec{B}_{meas} - \vec{B}_{int})^2 / N \right|^{1/2} \qquad (13)$$

$$|\Delta\vec{B}|_{res} = \left| \sum_{i=1}^{N} (\vec{B}_{meas} - \vec{B}_{int} - \Delta\vec{B}_{model})^2 / N \right|^{1/2} \qquad (14)$$

where $\vec{B}_{int}$ is the IGRF 1965.0 model of the internal field, $\Delta\vec{B}_{model}$ is given by Equations 7-9, and the quantities within the parentheses are vector differences, not differences between scalar magnitudes, as might be given if only scalar measurements were available. The summations are over the N bucket averages for each subset of the data.

As might be expected, $|\Delta\vec{B}|_{rms}$ increases with increasing magnetic activity, the measured difference field being about twice as great for periods when $Kp \geq 3$ as when $Kp = 0$ or 0^+. The residuals calculated with the appropriate models increase more or less proportionally. A figure of merit, defined by

$$F = \left|\Delta\vec{B}\right|_{res} / \left|\Delta\vec{B}\right|_{rms} \qquad (15)$$

which is a rough measure of the goodness of fit, is relatively constant at about 0.5. Thus, only about half of the measured vector difference field can be predicted by the appropriate model. We believe that time variations in the magnetospheric field are responsible for most of the residuals. Since dynamic changes are continually taking place within the magnetosphere, measurements made at different times at the same spatial position with the same tilt angle and Kp value would most likely yield values of the vector field differing among themselves by amounts roughly comparable to the residuals given in Table 3. Thus, it is our opinion that even if reliable measurements were available throughout the entire magnetosphere during all seasons of the year, and even if a model were used containing many more terms than these models, the figure-of-merit F could not be reduced much below the values given in Table 3. A model of the internal field such as that of Cain and Sweeney (1970) fits the scalar field in the altitude range 400-1500 km (where $|B|$ = 20,000-40,000γ) with an rms scalar residual of 9γ. It would appear that time variations throughout the magnetosphere, even during quiet times, are of the order of 10γ, and this represents about the limiting accuracy of any model which attempts to represent the average field configuration within the magnetosphere.

It is instructive to review the effect which changes in the form of the model have upon the root-mean-square residuals. We take the 17-coefficient MF73Q model as a base with which to compare the residuals obtained with other possible models. This model includes all terms

through quadratic in the spatial variables and linear in the tilt angle which satisfy the symmetry requirements of Equations 1-6. Restricting this model to only linear terms (7 coefficients) increased the residuals by 24%. A 60-coefficient quadratic model with both symmetric and asymmetric terms gave residuals 4% lower than the symmetric model. A 30-coefficient quadratic model without any dependence on tilt angle gave residuals 30% higher than the 17-coefficient model. A 33-coefficient model which permitted all symmetric terms through cubic in the spatial variables and linear in the tilt angle reduced the residuals by 6%. However, this cubic model exhibited a number of very unphysical characteristics in regions of 4-dimensional (X, Y, Z, T) space for which no data was available.

Thus the 17-coefficient symmetric quadratic model, with coefficients restricted so as to satisfy the $\vec{\nabla} \cdot \vec{B} = 0$ condition, has the best overall characteristics of any of the models we have derived to date. It is quite clear that any accurate model of the magnetospheric field must include a dependence upon tilt angle and must reflect in some fashion the presence of distributed currents. It seems that a quadratic model is the highest-order realistic model that can be derived from the present data set. Before higher-order models are feasible, additional data coverage is required: more measurements at very high latitudes, more complete distributions of data in longitude at all tilt angles, and vector measurements over a wide latitude range at distances less than 4 R_E.

MODEL CHARACTERISTICS

Representative field lines (every 2^O in latitude) for each of the

four models in the noon-midnight meridian (more specifically, in the

plane of symmetry rotated 4° from the noon-midnight meridian) for tilt

angle $T = 0^O$ are shown in <u>Figure 2</u>. Contours of constant total field

magnitude are shown as dashed lines. There is a marked tendency during

periods of high Kp for the equatorial crossing distance of the last

closed field line on the noon meridian to be closer to the earth and for

additional high-latitude lines to be swept back into the tail. In the

super-quiet (SQ) model the 76° line crosses the equator at 11.3 R_E and

the 80° line at 12.1 R_E on the dayside. In the super-disturbed (SD)

model, the 76° line crosses at 10.4 R_E and the 78° and 80° lines are

carried back into the tail. Thus, it appears that one effect of magnetic

disturbance is to transport magnetic flux from the dayside back into the

tail. The dayside latitude at the earth's surface separating the closed

field lines from the polar cap lines is generally about 5° lower than that

found in previous theoretically derived quantitative models, but is in

good agreement with the experimental results of <u>Fairfield</u> (1968).

In each model there are two high-latitude neutral points in the

noon meridian which separate those field lines which remain on the dayside

from those that are swept back into the tail. These neutral points move

closer to the earth and towards lower latitudes during periods of greater

magnetic disturbance. In the SQ model they are located at $\lambda_m = 62^O$,

$R = 13.5$ R_E, and in the SD model at $\lambda_m = 50^O$, $R = 11.3$ R_E. This compares

with a neutral point latitude of about 72° in the theoretical model of

Mead (1964) and 74° in the Olson (1969) and Choe et al. (1973) models,

independent of solar wind intensity.

An unexpected characteristic of each of the models is a minimum

in the field magnitude ($<10\gamma$) at around 12-15 R_E along the midnight

equator, beyond which the field strength begins to increase. We believe

that this is a non-physical characteristic, caused by the sparsity

of magnetometer data near the equatorial plane, together with the fact

that the expansions are only quadratic in the spatial variables and

contain no explicit terms which would represent the effects of a current

sheet in the tail.

Figure 3 shows the noon-midnight topology and field magnitude

contours for a tilt angle of 30°, corresponding to northern hemisphere

summer. Here again there is a strong tendency during periods of enhanced

magnetic activity for the last closed field line to be closer to the

earth and for more field lines to be swept back into the tail. As is

the case with almost all other tilted magnetosphere models, some of the

field lines appear to penetrate the dayside magnetopause, as though they

were connected with the interplanetary field.

One very clear effect is the change in latitude of the conjugate

point which takes place near solstice. The dayside field line emerging

at $+76^O$ for $T = 30^O$, for example, re-enters the earth at a latitude of

-73.3^O in the SQ model and -71.4^O in the SD model. Thus, the dayside

conjugate point in the winter hemisphere moves equatorward, sometimes

as much as 500-600 km. In the MF73D model the 78° line in the summer

hemisphere closes on the dayside, whereas both the 76° and 78° lines in the winter hemisphere are swept into the tail, and the 74° line appears to penetrate the magnetopause.

The effect is not as great on the nightside. For $T = 30^O$ the southern (winter) points conjugate to the $+66^O$ and $+68^O$ lines move about one or two degrees _poleward_ in the various models. Field lines originating at 70° latitude and above trace beyond 20 R_E in the tail, where the models are no longer applicable. Conjugate point variations at the synchronous orbit are discussed by Fairfield and Mead (1973).

A broad minimum in the field magnitude ($|B| < 10\gamma$) is located about midway between the solar magnetic and solar magnetospheric equators in the midnight meridian. There is again a (non-physical) tendency for the field magnitude to increase in value beyond 13-15 R_E in the midnight equatorial region. The neutral points are retained in the noon meridian, but the winter hemisphere neutral points move towards lower latitudes. In the SD model the winter hemisphere neutral point (for $T = 30^O$) moves from 50° down to 41° magnetic latitude, and the summer hemisphere neutral point moves up to 56° and inwards to 10.6 R_E. These latitudes are substantially lower than those obtained by Olson (1969) or Choe et al. (1973). The winter hemisphere neutral point in the model of Choe et al. moved from 74° down to 64° for $T = 30^O$; Olson found essentially no change in the magnetic latitude of the winter hemisphere neutral point. In both of these studies, however, the winter hemisphere neutral point moved outward and the summer hemisphere point moved inward, by approximately the same relative amount indicated in the present models. The substantially lower

latitude of the neutral points exhibited by the present models is probably another effect of the distributed currents within the magnetosphere, an effect which has been ignored in the various theoretically-derived models.

Figure 4 shows field line projections in the dawn-dusk meridian for the quiet and disturbed models and tilt angles of 0° and 30^0. Substantial shifts in the high-latitude conjugate points occur for $T = 30^O$. In general, the conjugate point in the winter hemisphere moves in longitude towards the midnight meridian. The line emerging at $+68^O$ latitude, $\pm90^O$ solar magnetic longitude, for example, re-enters the earth at a longitude of $\pm96.7^O$ for the SQ model and $\pm108^O$ for the SD model. There is very little shift in conjugate latitude, however.

Figure 5 shows the field lines as viewed from above and projected into the equatorial plane for the quiet and disturbed models. As with previous field models, the field lines tend to be swept back into the tail, the effect increasing rapidly with increasing latitude. This effect is substantially greater at any given latitude than that predicted by the theoretical model of Mead (1964); compare his Figure 8), but is consistent with the experimental results presented by Fairfield (1968). It is likely that currents within the magnetosphere contribute substantially to this enhanced sweeping effect.

Contours of the scalar difference $\Delta B = |B|_{model} - |B|_{dipole}$, together with the field-line topology in the noon-midnight meridian plane, are shown in Figure 6 for the quiet and disturbed models and for $T = 0^O$ and 30°. These may be compared with the experimentally-determined ΔB contours given by Sugiura (1972a, Figure 1) and Sugiura et al. (1971,

Figures 1, 3), except that those studies did not attempt to determine the effect of varying tilt angle. Four general regions can be identified: (1) a +ΔB region of about 20-30γ near the subsolar point; (2) a -ΔB region of 20-30γ near the neutral points on the dayside, agreeing generally with the results of Fairfield and Ness (1972); (3) a high-latitude +ΔB region of 30-50γ on the nightside; and (4) a tongue-like -ΔB region of 10-25γ near the equator on the nightside. The general pattern agrees quite well with the results of Sugiura et al. except that they find a more intense and highly localized -ΔB region near the magnetic equator inside 5 R_E on both the dayside and the nightside, reaching -35γ even during quiet times. This feature is not evident in our models because: (1) no data was used in our study inside 4 R_E, and most of the data between 4 and 6 R_E was taken at high latitudes; and (2) our simple quadratic models are not capable of describing an extremely localized region of intense -ΔB. The high-latitude +ΔB regions on the nightside, however, is reproduced quite well by our models. For large tilt angles such as $T = 30^O$, the +ΔB regions are much more intense in the summer hemisphere, reaching 60-70γ, than in the winter hemisphere, where ΔB is only about 20-40γ. The B contours given by these models are much more realistic than those given by the Mead-Williams model (see Sugiura et al., 1971, Figure 5).

The ΔB contours in the dawn-dusk meridian are shown in Figure 7. A 10-15γ depression is present near the equator, together with a 15-30γ region of positive ΔB at higher latitudes and over the poles, which presumably connects with the high-latitude +ΔB region on the nightside.

These contours compare favorably with those of Sugiura et al. (1971,

Figures 2, 4) except for the intense -ΔB regions very near the equator.

Figure 8 shows the contours of constant total field magnitude in

the equatorial plane, as calculated with the quiet and disturbed model

for $T = 0^\circ$. As expected, the contours, which would be circles centered

at the earth for a dipole field, are displaced toward the sun, indicating

that the field is more intense on the dayside. The broad minimum on the

nightside ($|B| < 10\gamma$) is seen to extend around almost to the dawn and

dusk meridians. These contours may be compared with those given by

Fairfield (1968, Figure 2), which were derived primarily from Explorer 21

(Imp 2) data, except near the subsolar point, where Explorer 12 data was

used. One discrepancy between these figures is that the earlier work

gives field strengths near the subsolar point roughly 20γ higher than the

present work. A possible explanation of this discrepancy is that the

solar wind flux may have been unusually high when Explorer 12 was near the

subsolar point in 1961, thus producing magnetopause locations (Cahill and

Patel, 1967) closer to the earth than normal (Fairfield, 1971), and

leading to the higher field strengths in Fairfield's contours. If this

is so, the contours in Figure 9 are more typical in this respect. A

second discrepancy is the curvature of the contours near the dawn and dusk

meridians in Figure 8, a feature which does not appear in Fairfield's

contours. This curvature is probably an artificial effect, related to the

tendency of the Z-component to increase with increasing distance beyond

about 14 R_E. A third discrepancy is the presence of a steeper nightside

gradient near 7 R_E in Fairfield's contours. This may be a real effect,

which cannot be reproduced with our simple quadratic models.

Figure 9 shows the locus of the last closed field lines in the equatorial plane on the dayside for each of the four models for $T = 0^O$, together with the average magnetopause position as observed by Fairfield (1971). The calculated position for the two disturbed models agrees reasonably well with the observed magnetopause position. The last closed field line in the two quiet models, however, is 1-2 R_E outside the average observed magnetopause. The observations summarized by Fairfield (1971) were made over a wide range of tilt angles, whereas the model calculations were made with zero tilt. Calculations made with $T \neq 0^O$ were somewhat more difficult to interpret, since in some regions near the expected magnetopause a field line traced in one direction will intersect the earth, whereas in the other direction it is open (e.g., see the -76° and -78° field lines of the MF73SQ model in Figure 3). However, even if one defines the magnetopause as the locus of the outermost point in the solar magnetospheric equatorial plane where only one end of the field line intersects the earth, this locus falls earthward of the last closed field line for $T = 0^O$ except for a limited region near the subsolar point. Therefore, if one were to compute an average of the equatorial distance of the last closed field line over a range of tilt angles, this average would fall inside the corresponding $T = 0^O$ curves in Figure 9 and improve the agreement with the observations.

It should be stressed at this point that no constraints other than those of symmetry have been placed on the models to achieve the various results described in this section. No observed or calculated magnetopause

positions have been used to derive the models. The only input are the

vector magnetic field measurements inside the magnetopause expressed as

functions of X, Y, Z, T, and Kp. The position of the last closed field

line and neutral points on the dayside, the minimum field region in the

tail, the general alignment of field lines in the tail with the solar

wind direction, etc., all result from making least-squares fits to the

quadratic expansions. It is reassuring that the positions of the last

closed field lines on the dayside agree as well as they do with the

observed magnetopause positions. The agreement gives additional confidence

in the general validity of the models.

Figure 10 shows ATS-5 measurements by Skillman (1973) of the average

diurnal variation in the three components of the field during quiet times

at different seasons of the year. The satellite was in a synchronous

equatorial orbit at a longitude of 105° west of Greenwich, placing it at

a geomagnetic latitude of 9.3°. Also shown are the calculated values of

the three components, using the IGRF internal field plus the MF73Q model.

The calculated north or H component agrees quite well with the data for

all three seasons, except for the average magnitude. Since the H com-

ponent was along the satellite spin axis, the zero level was not precisely

known, and a different choice for zero level would bring theory and

experiment into better agreement. The predicted variation of the D or east

component agrees remarkably well with the measurements at all seasons. The

shape of the predicted vertical or V component differs somewhat from the

measurements, but the average level and separation by seasons are in general

agreement. Thus the model seems to predict the general characteristics of

the field at 6.6 R_E rather well.

The distributed magnetospheric currents implied by the models

are easily calculated by taking the curl of Equations 7-9, yielding

$$(\nabla \times \vec{B})_x = (2c_4 - b_1) \; Y \tag{16}$$

$$(\nabla \times \vec{B})_y = (a_1 - c_2) + (a_2 - 2c_3) \; X + (2a_7 - c_7) \; T \; Z \tag{17}$$

$$(\nabla \times \vec{B})_z = (b_3 - 2a_6) \; T \; Y \tag{18}$$

(The curl of the dipole field is, of course, zero.) The values of each

of these coefficients for the four models is given in Table 4. $\nabla \times \vec{B}$ is

in units of $\gamma/10R_E$ when the solar magnetic coordinates are in units of

tens of earth radii and T is in units of tens of degrees. By Maxwell's

equations the current density is given by $\vec{J} = \nabla \times \vec{B}/\mu_0$ where

$\mu_0 = 4\pi \times 10^{-7}$ newtons/amp^2 in rationalized mks units. Thus to obtain

the current density in amp/m^2 the right-hand-side of Equations 16-18

should be multiplied by 1.25×10^{-11}.

Note that for T = 0° Equations 16-17 imply that the currents

parallel to the equatorial plane are independent of Z and therefore not

restricted to the plasma sheet in the tail. This unrealistic feature

results from the fact that the field models contain only symmetric terms

through quadratic in the spatial variables, and therefore the currents

contain only linear terms.

The current system in the X-Y plane for T = 0° implied by the

MF73D model is shown in Figure 11. These currents are roughly concentric

about X = 2.5 R_E, Y = 0, and the current density increases linearly with

distance from this point. The large currents in the tail have a magnitude

of approximately $10\gamma/R_E \simeq 1.2\times10^{-9}$ amp/m^2. This is comparable to the

current densities obtained by Olson (1973). If the tail has a diameter

of approximately 30 R_E at this point, a rough calculation yields a value

of about 10^7 amperes for the total current flowing across the tail

between $X = -5$ and $X = -15$ R_E.

There is no indication of any ring currents near the

earth such as that indicated in the work of Sugiura (1972a, 1972b, 1973).

In principle, one should be able to determine the magnitude and extent

of such a ring current by taking the curl of experimentally-derived

models such as these. However, much more sophisticated models would

have to be used in order to provide high-order terms in the $\vec{V}\times\vec{B}$ expression

appropriate to the geometry of such a ring current. The present

expressions, containing only linear terms, are limited to determining

only the gross current patterns in the outer magnetosphere.

MODEL LIMITATIONS

A number of factors limit the accuracy and usefulness of these models. First of all, no data beyond 17 R_E was used as input to define the models. Therefore, the models should not be used to calculate fields beyond 17 R_E. Otherwise, unreliable results are likely to be obtained.

Secondly, there are large gaps in the data coverage. As indicated in an earlier section, 70% of the four-dimensional buckets contain no data. This lack of coverage is particularly evident at very high latitudes (especially high southern latitudes), at near-equatorial latitudes, and at distances less than 5 R_E. There is also a lack of coverage at certain longitudes during some seasons of the year. The models may be inaccurate in these regions, just as models of the internal field based on surface measurements are likely to be inaccurate over large ocean and polar cap regions where little or no data are available.

Thirdly, the present models cannot represent asymmetries in the magnetosphere. Only terms which satisfy the symmetry requirements of Equations 1-6 have been included. The models may therefore be suppressing real asymmetries, such as the several-degree dawn-dusk asymmetries in declination recently reported by Sugiura (1973). This particular asymmetry can be seen in our experimental data, but is suppressed by the models.

Fourth, insufficient terms have been included in the models to represent the effects of relatively localized current systems. This is particularly true in the case of the near-earth equatorial ring current and sheet currents in the tail. Attempts to add higher-order

terms (for example, a 33-coefficient cubic model) gave rise to undesirable characteristics in regions where there was no data. Better data coverage is necessary before significant extensions of this type can be made.

Finally, the models can only represent an average magneto-spheric configuration. Models such as these cannot represent the rapid time variations in magnetospheric configuration which take place during substorms. Such an extension to include time variations would obviously be highly desirable, but is undoubtedly far in the future.

Despite these limitations,we believe that these models repre-sent the average field in the region from 4-17 R_E more accurately than any other model presently available. They have the additional advantage of being extremely simple to use; the FORTRAN decks representing the models are extremely short and require insignificant amounts of computer time to make a field calculation. Although other models exist which include either the effect of distributed currents or the effect of changes in the tilt angle, none contain both, and we feel that both effects must be included in any realistic model of the outer magnetospheric field.

APPENDIX: COORDINATE SYSTEMS

Equations 7-9 require as inputs solar magnetic coordinates and tilt angle. In many practical applications, however, the coordinates which are readily available are geographic latitude and longitude, day of year, and either Universal Time (UT) or local time. In addition, one frequently wishes to use an internal model such as the IGRF (IAGA, 1969) together with these external models, rather than a simple dipole model. One must be careful in such cases to use a consistent coordinate system. Our preference is to make all such calculations in a geomagnetic dipole coordinate system, with the Z-axis parallel to the magnetic dipole. Appropriate formulas to transform spatial coordinates from geographic to geomagnetic latitude and longitude and vice versa are given by Mead (1970). The declination of the sun δ_S can be obtained from ephemeris tables, or an algorithm such as Mead's given in Russell (1971); however, where high accuracy is not needed, the following algorithms are useful:

$$\sin \delta_S = \sin \varepsilon \sin \lambda_S \qquad (A1)$$

$$\lambda_S \simeq 360 \; (IDAY - 81.6)/365.25 \qquad (A2)$$

where $\varepsilon = 23.44^\circ$ is the obliquity of the ecliptic, λ_S is the sun's celestial longitude along the ecliptic, and IDAY is the day of the year, with January 1 being day 1. The declination given by these algorithms, which assume that the sun moves uniformly along the ecliptic, is accurate to about half a degree.

The tilt angle T, equal to the geomagnetic latitude of the sun, is defined by

$$\sin T = \cos 11.4^O \sin \delta_s + \sin 11.4^O \cos \delta_s \cos (GHA_s - 69.8^O) \qquad (A3)$$

where GHA_s is the Greenwich hour angle of the sun, given by

$$GHA_s = GST - \alpha_s \simeq 15 * UT - 180^O \qquad (A4)$$

where GST is Greenwich Sidereal Time and α_s is the sun's right ascension. The position of the dipole (11.4^O colatitude, 69.8^O west longitude) is that given by the IGRF model at epoch 1965.0 (Mead, 1970). Solar magnetic latitude is the same as geomagnetic latitude. Solar magnetic longitude is the same as magnetic local time (MLT) ± 12 hours. It is equal to the geomagnetic longitude, measured eastward from the dipole meridian, plus the magnetic hour angle of the sun, measured westward from the dipole meridian. The sun's magnetic hour angle MHA_s is defined by

$$\sin MHA_s = \cos \delta_s \sin (GHA_s - 69.8^O) / \cos T \qquad (A5)$$

$$\cos MHA_s = (\cos 11.4^O \sin T - \sin \delta_s) / (\sin 11.4^O \cos T) \qquad (A6)$$

Equations A1-A6 plus those given by Mead (1970) can be used to calculate the solar magnetic coordinates and tilt angle needed as input to Equations 7-9. The internal field for the IGRF model can be obtained by using the coefficients given by Mead (1970) or Stern (1971) for input in magnetic dipole coordinates. (Fortran decks which include all these calculations are available from the authors.)

Calculations of seasonal and diurnal variations of geomagnetic

phenomena must take into proper consideration the coherent variation

of the tilt angle with local time during a 24-hour day. This coherence

will depend upon the geomagnetic longitude of the observer. At a dipole

longitude of 0° (69.8^O west geographic longitude) the tilt angle will be

a maximum at noon and a minimum at midnight. The maximum and minimum

are reversed at 180° geomagnetic longitude, and a different phase

relationship will exist at other longitudes. Thus even if a dipole is

used for the internal field, the calculated diurnal variations of such

phenomena as conjugate point positions will depend on the geomagnetic

longitude of the observer as well as on the latitude and season of the

year.

ACKNOWLEDGMENTS

REFERENCES

Antonova, A. Ye., and V. P. Shabanskiy, Structure of the geomagnetic

   field at great distances from the earth, Geomagnetism and Aeronomy,

   8, 639-647, 1968.

Behannon, Kenneth W., Mapping of the earth's bow shock and magnetic

   tail by Explorer 33, J. Geophys. Res., 73, 907-930, 1968.

Cahill, L. J., Jr., and V. L. Patel, The boundary of the geomagnetic

   field, August to November 1961, Planet. Space Sci., 15,

   997-1033, 1967.

Cain, J. C., and R. E. Sweeney, Magnetic field mapping of the inner

   magnetosphere, J. Geophys. Res., 75, 4360-4362, 1970.

Choe, J. Y., and D. B. Beard, The geomagnetic field deduced from

   magnetopause currents, submitted to Planet. Space Sci., 1973.

Choe, J. Y., D. B. Beard, and E. C. Sullivan, Precise calculation of

   the magnetosphere surface for a tilted dipole, Planet. Space Sci.,

   21, 485-498, 1973.

Cummings, W. D., P. J. Coleman, Jr., and G. L. Siscoe, Quiet Day Magnetic

   Field at ATS 1, J. Geophys. Res, 76, 926-932, 1971.

Fairfield, D. H., Average magnetic field configuration of the outer

   magnetosphere, J. Geophys. Res., 73, 7329-7338, 1968.

Fairfield, D. H., Bow shock associated waves observed in the far upstream

   interplanetary medium, J. Geophys. Res., 74, 3541-3553, 1969.

Fairfield, D. H., Average and unusual locations of the earth's

   magnetopause and bow shock, J. Geophys. Res., 76, 6700-6716,

   1971.

Fairfield, D. H., Whistler waves upstream from collisionless shocks,
    submitted to J. Geophys. Res., 1973a.

Fairfield, D. H., Magnetic field signatures of substorms on high-
    latitude field lines in the nighttime magnetosphere, J. Geophys.
    Res., 78, 1553-1562, 1973b.

Fairfield, D. H., and G. D. Mead, Magnetospheric mapping with quantitative
    geomagnetic field models, submitted to J. Geophys. Res., 1973.

Fairfield, D. H., and N. F. Ness, Magnetic field measurements with
    the IMP 2 satellite, J. Geophys. Res., 72, 2379-2402, 1967.

Fairfield, D. H. and N. F. Ness, IMP 5 magnetic field measurements in
    the high latitude outer magnetosphere near the noon meridian,
    J. Geophys. Res., 77, 611-623, 1972.

Hones, E. W., Jr., Motion of charged particles trapped in the
    earth's magnetosphere, J. Geophys. Res., 68, 1209-1219, 1963.

IAGA Commission 2, International Geomagnetic Reference Field 1965.0,
    J. Geophys. Res., 74, 4407-4408, 1969.

Mead, G. D., Deformation of the geomagnetic field by the solar wind,
    J. Geophys. Res., 69, 1181-1195, 1964.

Mead, G. D., Neutral points on the boundary of the closed magnetosphere,
    Space Sci. Rev., 7, 158-165, 1967.

Mead, G. D., International geomagnetic reference field 1965.0 in
    dipole coordinates, J. Geophys. Res., 75, 4372-4374, 1970.

Mead, G. D., and D. B. Beard, Shape of the geomagnetic field solar
    wind boundary, J. Geophys. Res., 69, 1169-1179, 1964.

Mead, G. D., and L. J. Cahill, Jr., Explorer XII measurements of the
distortion of the geomagnetic field by the solar wind, J. Geophys.
Res., 72, 2737-2748, 1967.

Midgley, J. E., Perturbation of the geomagnetic field--a spherical
harmonic expansion, J. Geophys. Res., 69, 1197, 1964.

Olson, W. P., The shape of the tilted magnetopause, J. Geophys. Res.,
74, 5642-5651, 1969.

Olson, W. P., The distributed magnetospheric currents, submitted to
J. Geophys. Res., 1973.

Olson, W. P., and K.A. Pfitzer, A quantitative model of the magnetospheric
magnetic field, submitted to J. Geophys. Res., 1973.

Roederer, J. G., Quantitative models of the magnetosphere, Rev. Geophys.,
7, 77-96, 1969.

Russell, C. T., Geophysical coordinate transformations, Cosmic
Electrodynamics, 2, 184-196, 1971.

Skillman, T. L., Average daily variations in the magnetic field as
observed by ATS-5, GSFC X-645-72-301, August 1972, NASA Technical
Note, in press, 1973.

Stern, D. P., Geomagnetic potential in dipole coordinates, J. Geophys.
Res., 76, 257-258, 1971.

Sugiura, M., Equatorial current sheet in the magnetosphere, J. Geophys.
Res., 77, 6093-6103, 1972a.

Sugiura, M., The ring current, in Critical Problems of Magnetospheric
Physics, edited by E. R. Dyer, pp. 195-210, National Academy of
Sciences, Washington, D. C., 1972b.

Sugiura, M., Quiet time magnetospheric field depression at 2.3-3.6 R_E, J. Geophys. Res., 78, 3182-3185, 1973.

Sugiura, M., Magnetospheric field morphology at magnetically quiet times, Radio Science, November 1973.

Sugiura, M., B. G. Ledley, T. L. Skillman and J. P. Heppner, Magnetospheric distortions observed by OGO 3 and 5, J. Geophys. Res., 76, 7552-7565, 1971.

Sugiura, M., and D. J. Poros, A magnetospheric field model incorporating the OGO 3 and OGO 5 magnetic field observations, Planetary Space Sci., 21, 1763-1773, 1973.

Taylor, H. E., and E. W. Hones, Jr., Adiabatic motion of auroral particles in a model of the electric and magnetic fields surrounding the earth, J. Geophys. Res., 70, 3605-3628, 1965.

Williams, D. J., and G. D. Mead, Nightside magnetospheric configuration as obtained from trapped electrons at 1100 km, J. Geophys. Res., 70, 3017-3029, 1965.

Table 1. Summary of the magnetometer data obtained

from the four Imp spacecraft.

Satellite	Time Interval	Total Time	No. of Orbits	No. of Individual Measurements	No. of $0.5R_E$ Averages
Explorer 33	7/66 – 7/68	356 hrs.	34	0.25×10^6	744
Explorer 34	5/67 – 2/69	1166	144	1.54×10^6	3510
Explorer 41	6/69 – 9/71	1920	195	2.60×10^6	5668
Explorer 43	3/71 – 3/72	898	78	40.37×10^6	2694
Totals		4340 hrs.	451	44.76×10^6	12616

Table 2. Values of the coefficients to be substituted into Equations 7-9 for each of the four models. The units are such that the contribution from each term is in gammas if the cartesian solar magnetic coordinates X, Y, and Z are in units of tens of earth radii and the tilt angle T is in units of tens of degrees.

Component	Coefficient	Term	Super-quiet MF73SQ $Kp=0,0^+$	Quiet MF73Q $Kp<2$	Disturbed MF73D $Kp \geq 2$	Super-Disturbed MF73SD $Kp \geq 3$
ΔB_x	a_1	Z	17.93	21.79	33.16	39.48
	a_2	XZ	-5.79	-7.03	-6.39	-2.91
	a_3	T	2.98	3.02	4.30	5.17
	a_4	TX	-2.57	-2.99	-3.25	-3.86
	a_5	TX^2	-0.30	-0.62	-0.44	-1.04
	a_6	TY^2	-1.47	-1.22	-1.27	-1.29
	a_7	TZ^2	1.05	0.95	0.45	-1.14
ΔB_y	b_1	YZ	-10.11	-11.84	-16.54	-19.10
	b_2	TY	-1.98	-2.57	-3.08	-3.50
	b_3	TXY	0.09	-0.28	0.22	0.23
ΔB_z	c_1	1	-9.41	-11.96	-19.88	-22.90
	c_2	X	15.07	17.87	20.23	22.70
	c_3	X^2	13.16	15.88	22.72	26.50
	c_4	Y^2	8.36	9.77	13.23	15.54
	c_5	Z^2	7.95	9.43	11.46	11.00
	c_6	TZ	4.55	5.57	6.33	7.36
	c_7	TXZ	0.51	1.53	0.67	1.85

Table 3. Root-mean-square values of the measured vector
difference field $|\Delta\vec{B}|_{rms}$, the vector residual
field $|\Delta\vec{B}|_{res}$ and the figure-of-merit F (see
text for definition), for each of the four models.

	$|\Delta\vec{B}|_{rms}$	$|\Delta\vec{B}|_{res}$	F
MF73SQ	17.4	8.2	0.47
MF73Q	20.8	10.1	0.49
MF73D	29.9	15.9	0.53
MF73SD	34.8	18.8	0.54

Table 4. Coefficients for $\vec{\nabla \times B}$ in Equations 16-18.
See text for discussion of units.

Coefficients	MF73SQ	MF73Q	MF73D	MF73SD
$2c_4 - b_1$	26.83	31.38	43.00	50.18
$a_1 - c_2$	2.86	3.92	12.93	16.78
$a_2 - 2c_3$	-32.11	-38.79	-51.83	-55.91
$2a_7 - c_7$	1.59	0.37	0.22	-4.13
$b_3 - 2a_6$	-3.03	-2.16	-2.76	-2.81

FIGURE CAPTIONS

Figure 1. Distribution of the data set in four-dimensional coordinate space. The top half shows the distribution at 6-8 R_E and the bottom half at 13-15 R_E. The symbols indicate the range of the tilt angle associated with each measurement.

Figure 2. Field lines and contours of constant total field magnitude in the noon-midnight meridian for $T = 0^O$. Field lines are plotted every 2^O in latitude, beginning with 66°. Contours are given every 10γ from $10-100\gamma$. North-south symmetry is built into the models. Field lines and contours are terminated beyond 20 R_E.

Figure 3. Same as Figure 2, but for $T = 30^O$. The symmetry is such that the northern and southern hemispheres would be exactly reversed for $T = -30^O$.

Figure 4. Field-line projections in the dawn-dusk meridian for $T = 0^O$ and $T = 30^O$. The field lines tend to be swept back into the tail. The view is along the solar magnetic equator.

Figure 5. Field lines from rings of constant latitude, as viewed from above and projected into the equator. Lines are shown for every two hours of local time. Due to the basic symmetry of the models, the southern portion of each closed field line exactly overlaps the northern portion, and many of the lines which appear open are actually closed. Field lines from two models are plotted together; the lines from the MF73D model are always swept back further towards the tail.

Figure 6.   Contours of constant $\Delta B = |B|_{total} - |B|_{dipole}$, superimposed on the noon-midnight field topology.   Contours are shown in 10γ intervals.

Figure 7.   Contours of constant ΔB in the dawn-dusk meridian for $T = 0^{\circ}$ and $T = 30^{\circ}$.

Figure 8.   Contours of constant total field magnitude in the equatorial plane for $T = 0^{\circ}$.   Contours are given every 10γ from 10γ-100γ.   The apparent increase in field magnitude beyond 13 R_E is probably not a real effect.

Figure 9.   Contours of the last closed field line in the equatorial plane given by the four models for $T = 0^{\circ}$, plus the average position as observed by Fairfield (1971).

Figure 10.   Diurnal and seasonal variation of the field at synchronous orbit.   On the left are measured quiet-time averages obtained by Sugiura (1973) on ATS-5, located at a longitude of -105°. On the right are the values predicted by the MF73Q model at equinox and summer and winter solstice.   The base line for the three components is that given by the IGRF internal model.

Figure 11.   Curl B in the equatorial plane for $T = 0^{\circ}$ (MF73D model).   To get current densities in amp/m^2, multiply the curl in γ/R_E by 1.25×10^{-10}.
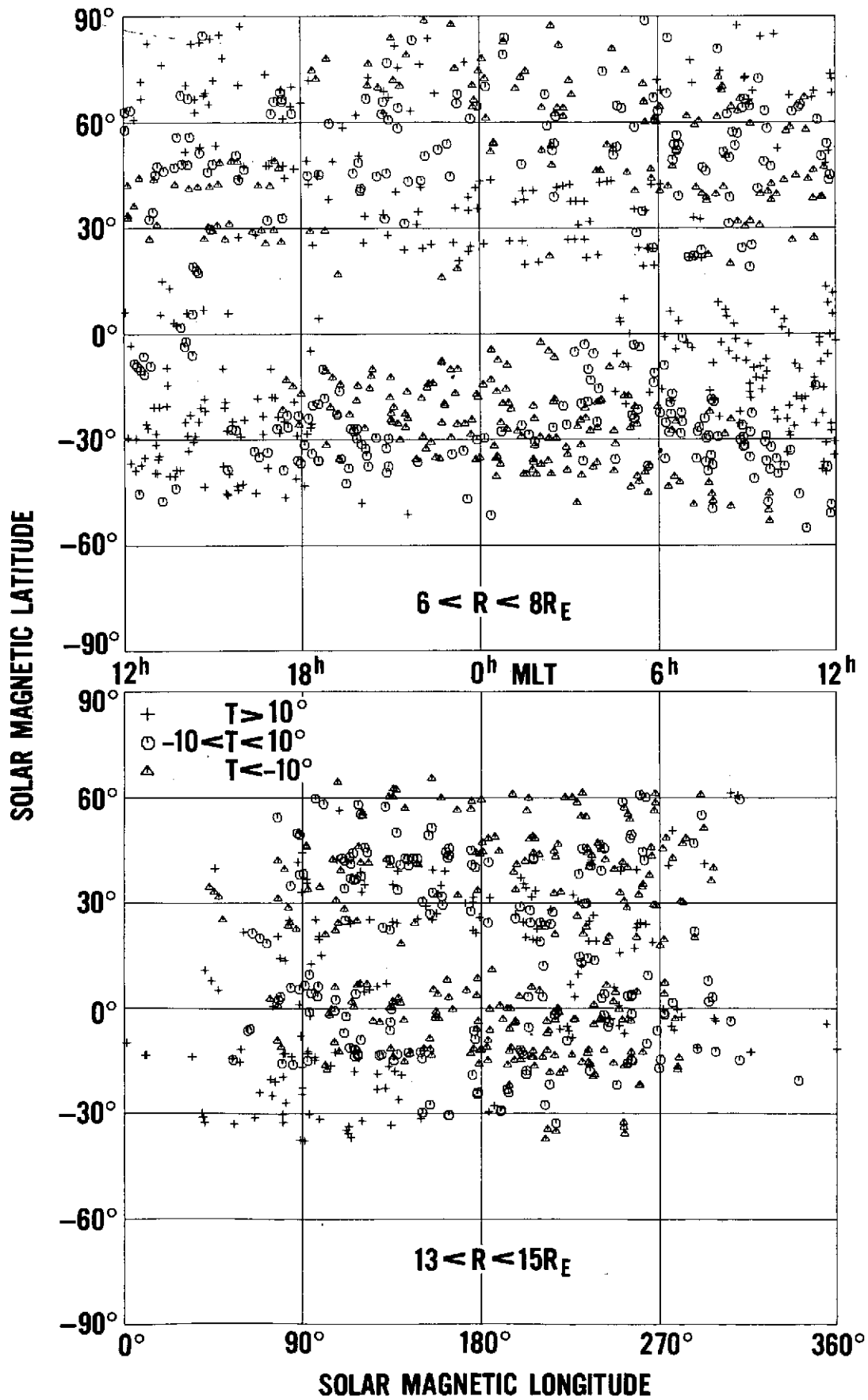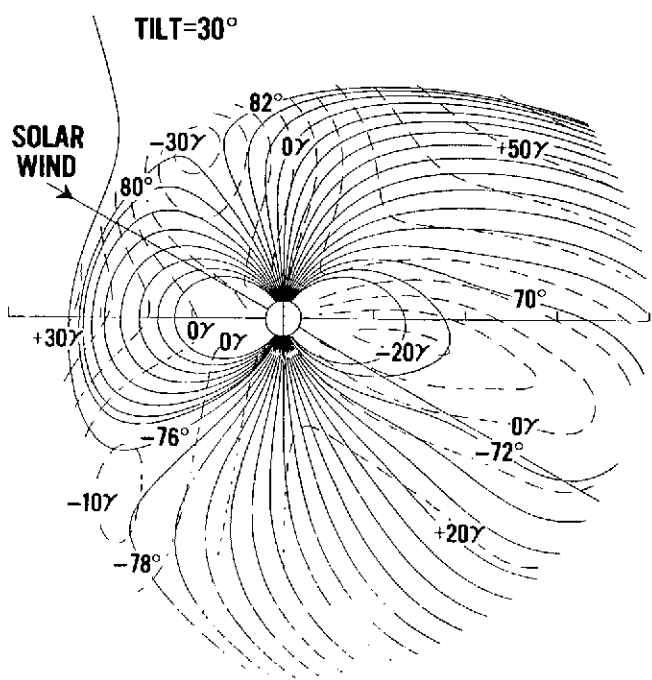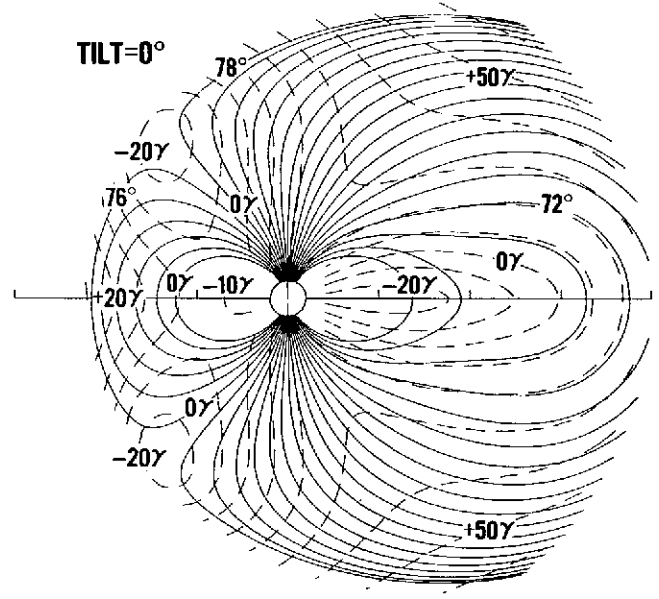
Figure 1.
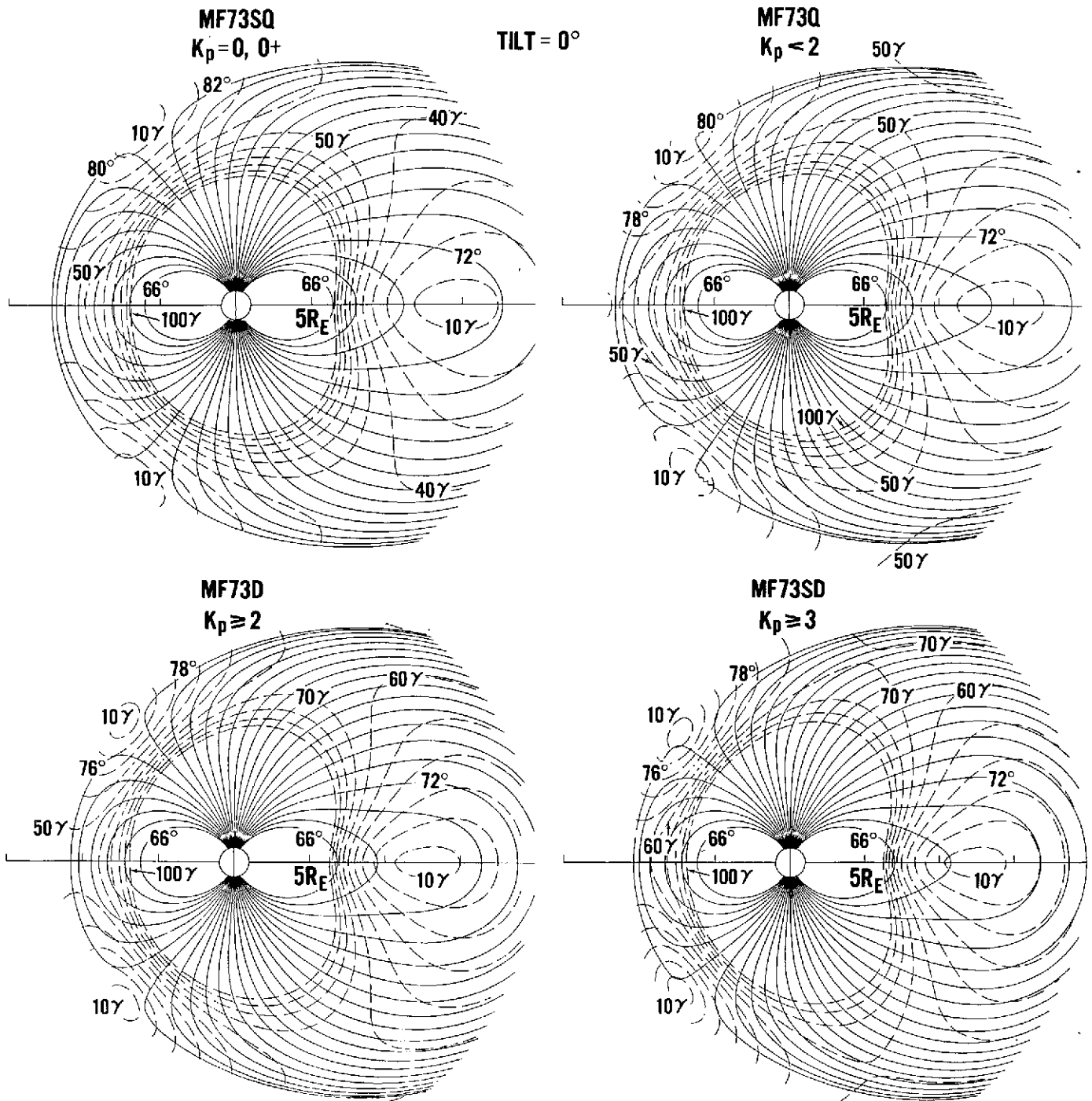
Figure 2
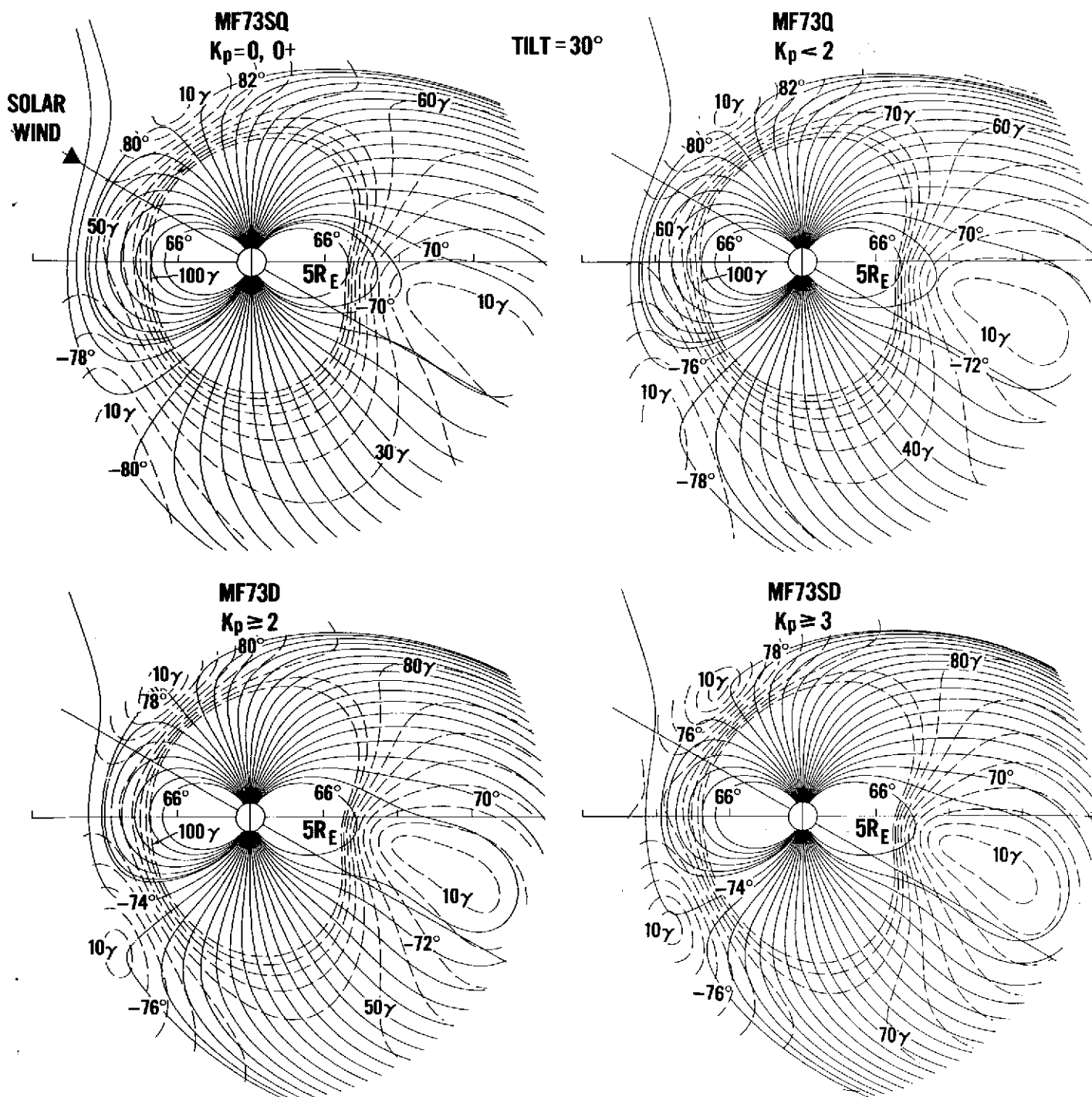
Figure 3
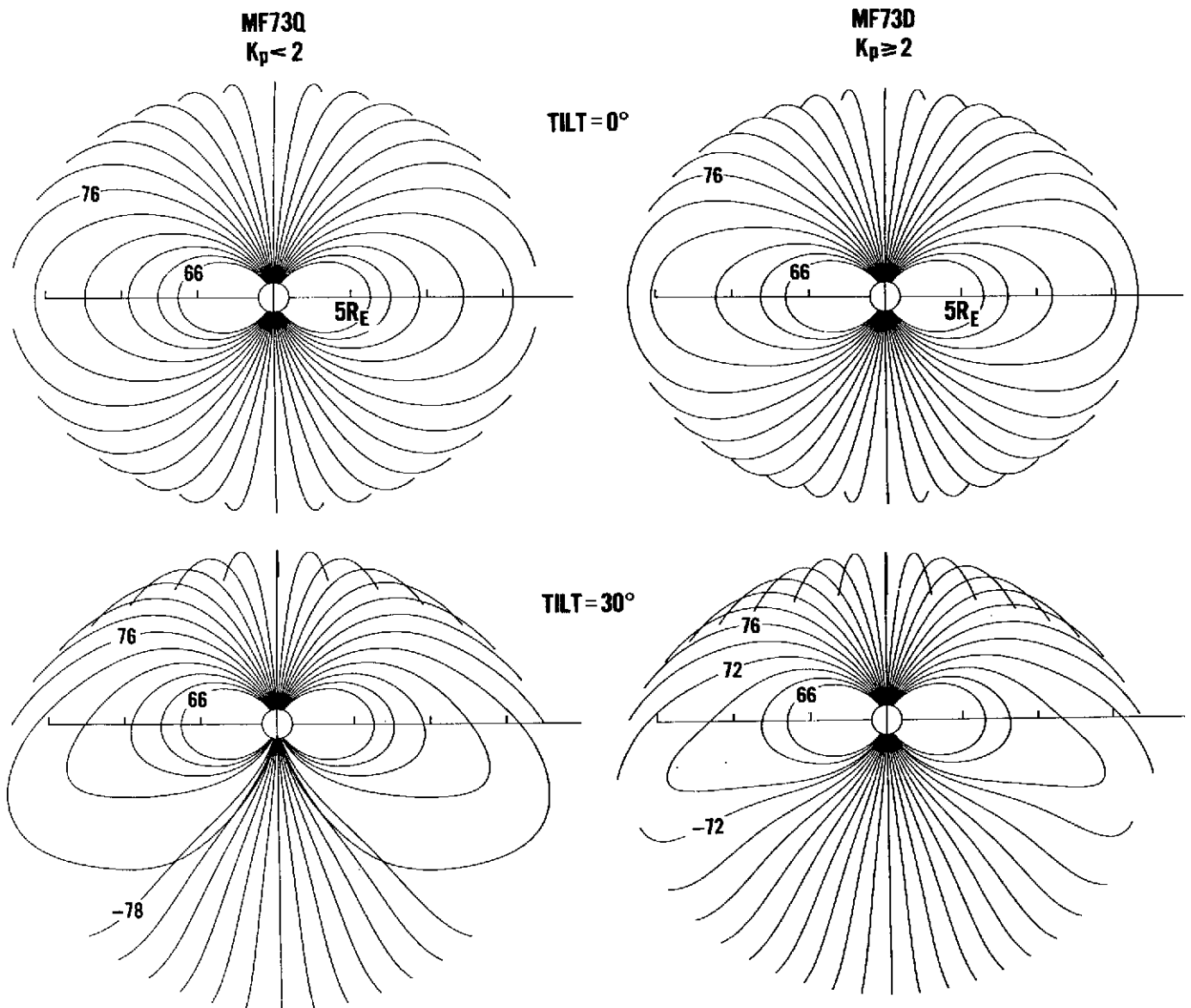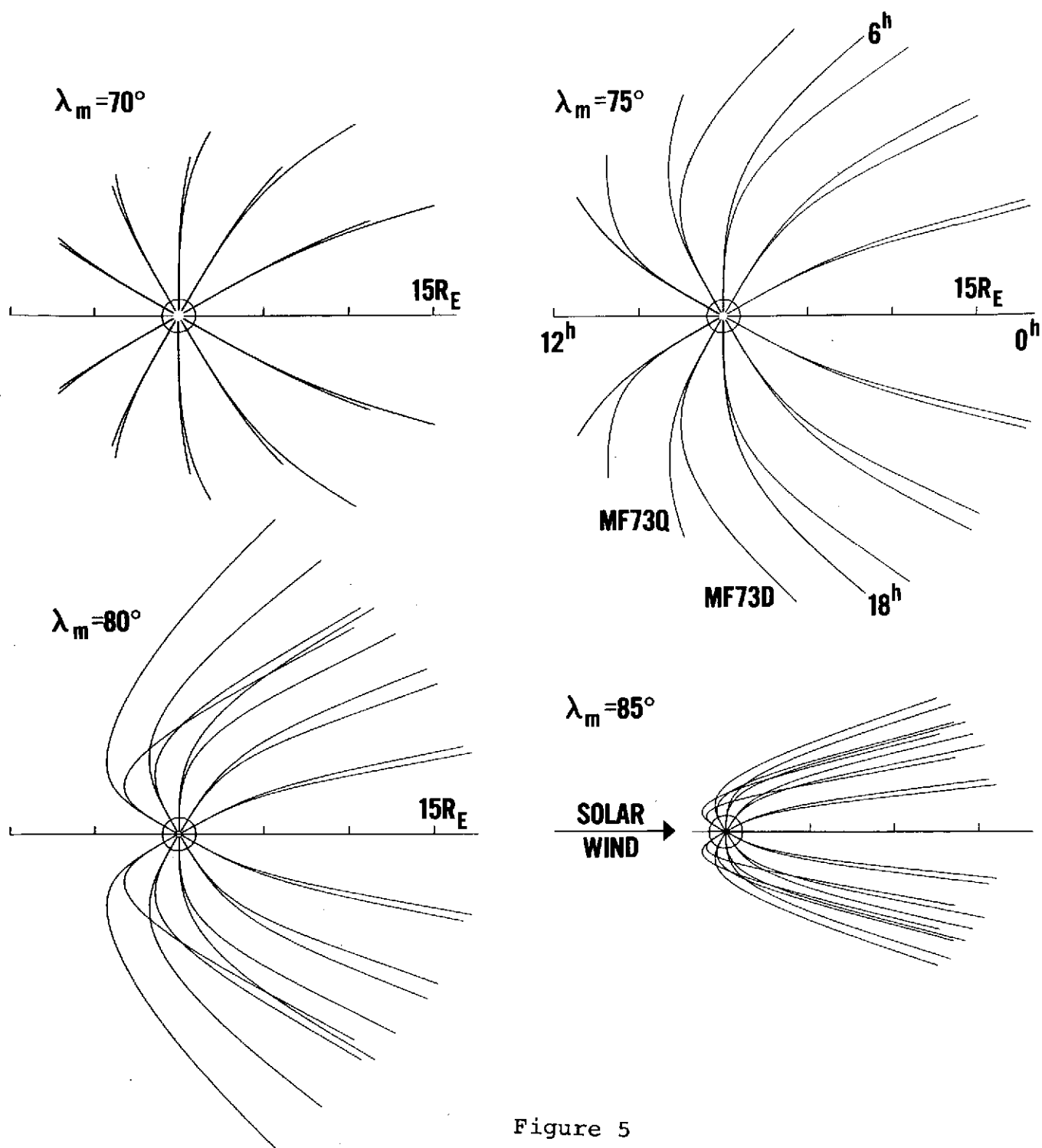
MF73Q
$K_p < 2$

MF73D
$K_p \geq 2$

TILT = 0°

5R$_E$

76

66

76

66

5R$_E$

TILT = 30°

76

66

76

72
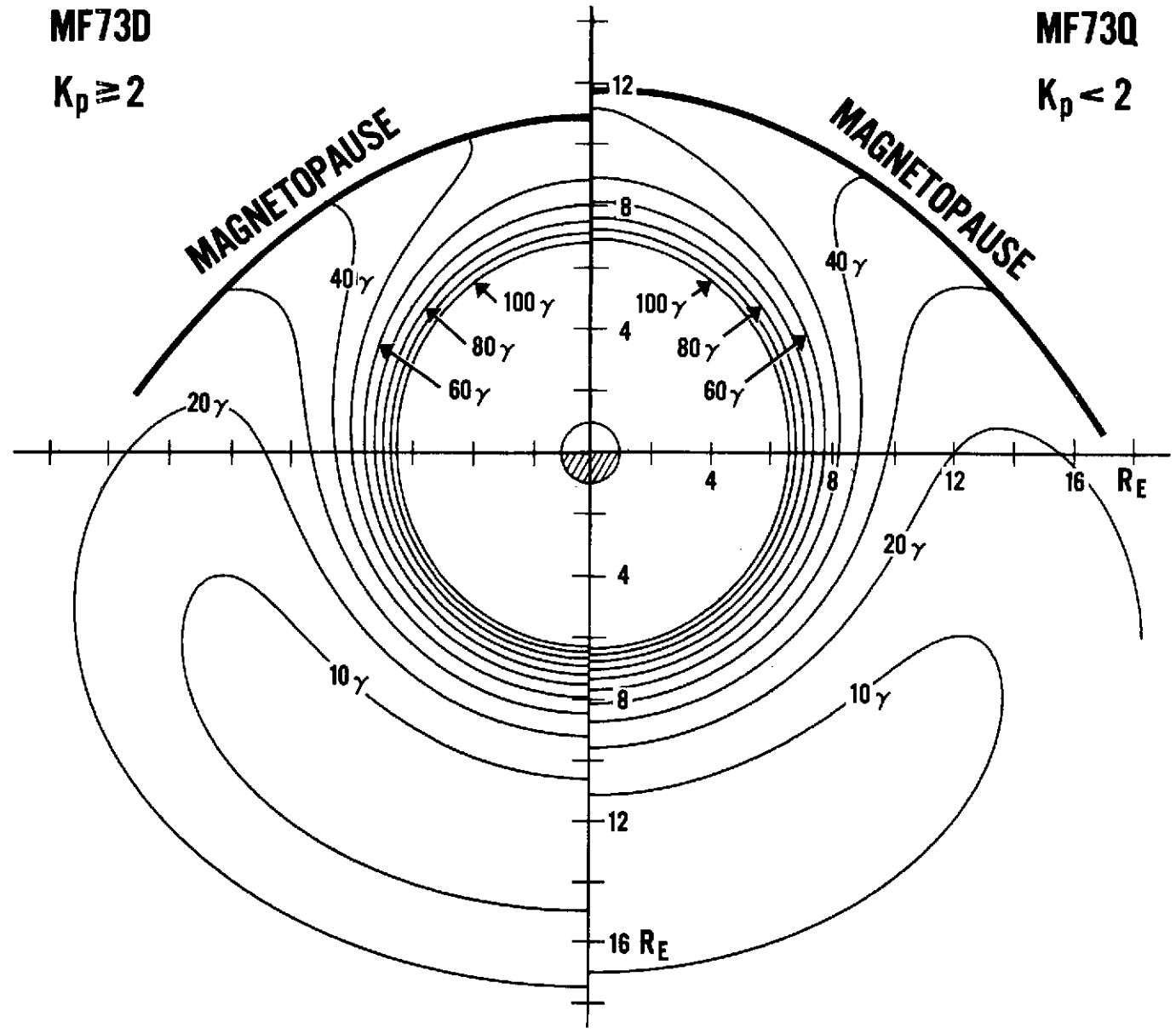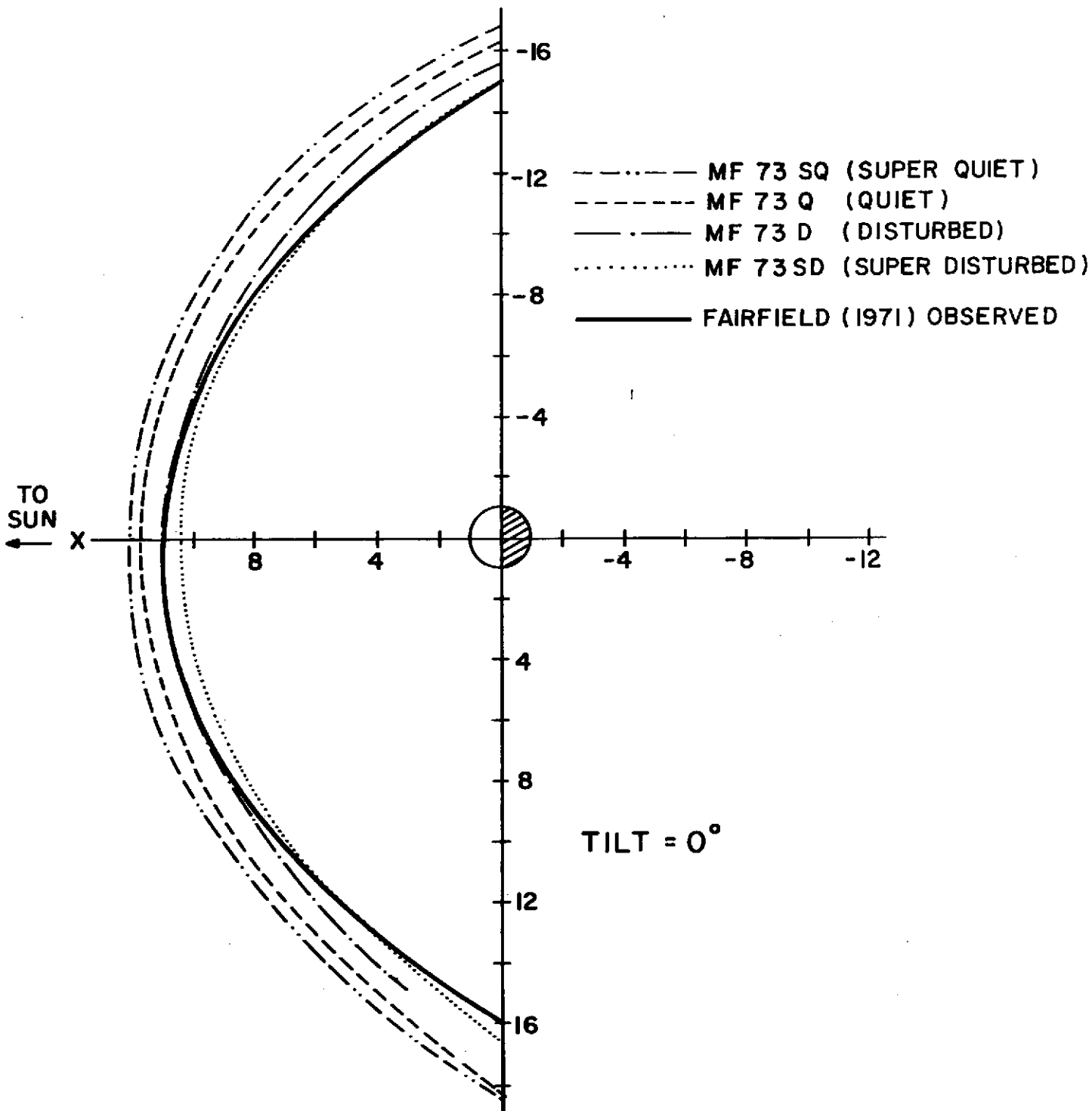
66

−78

−72
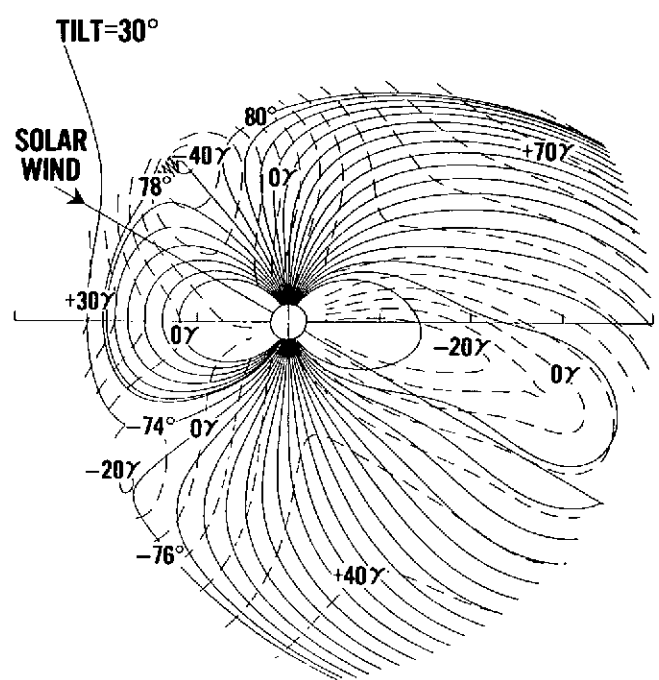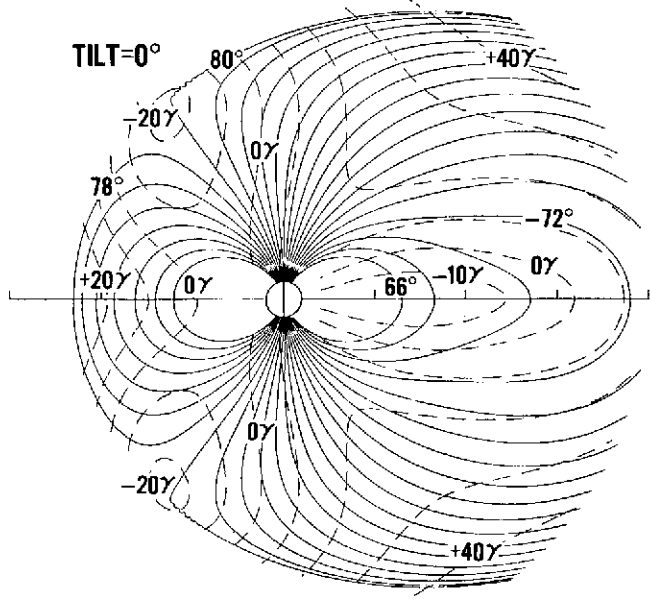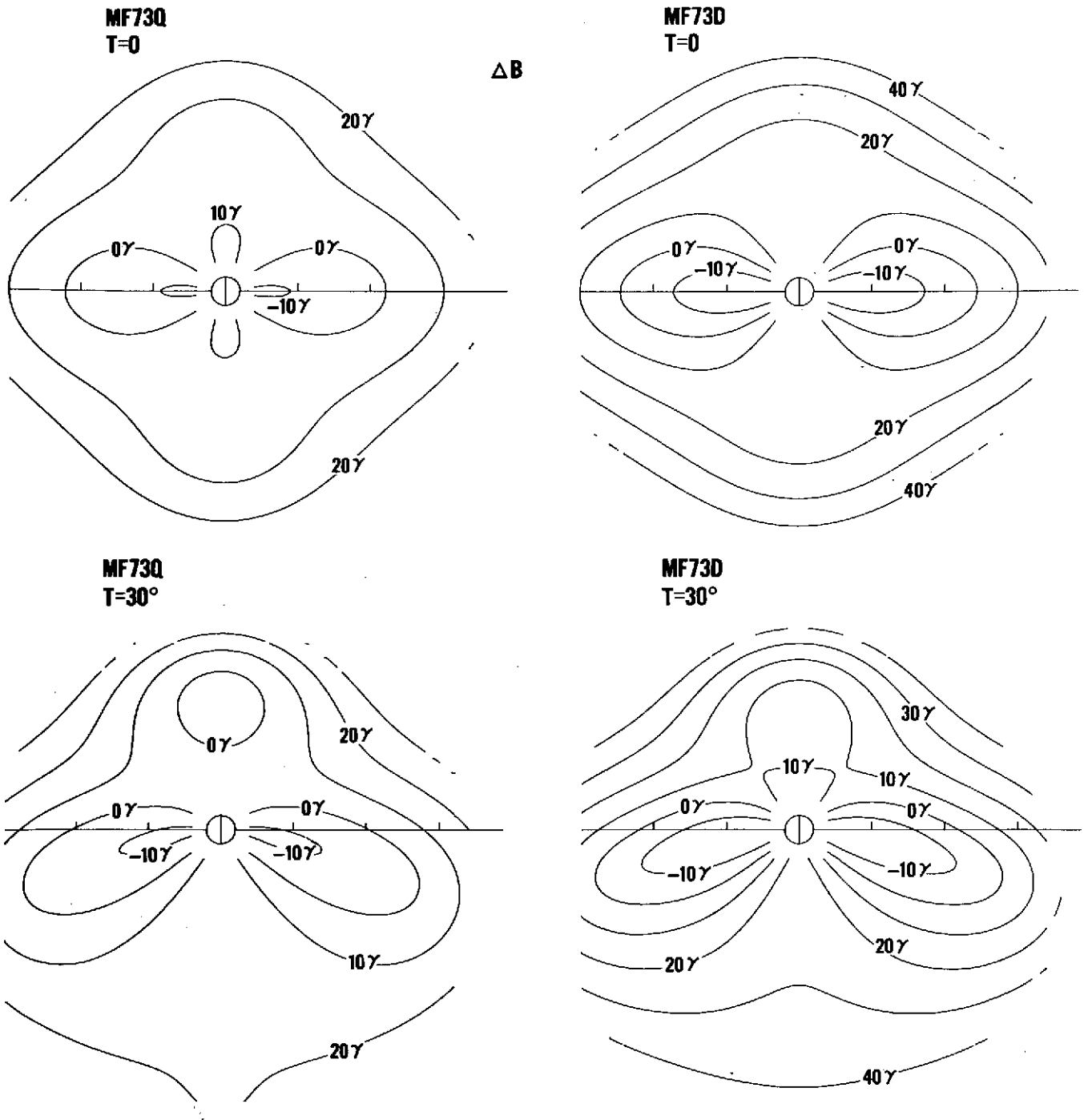
Figure 4

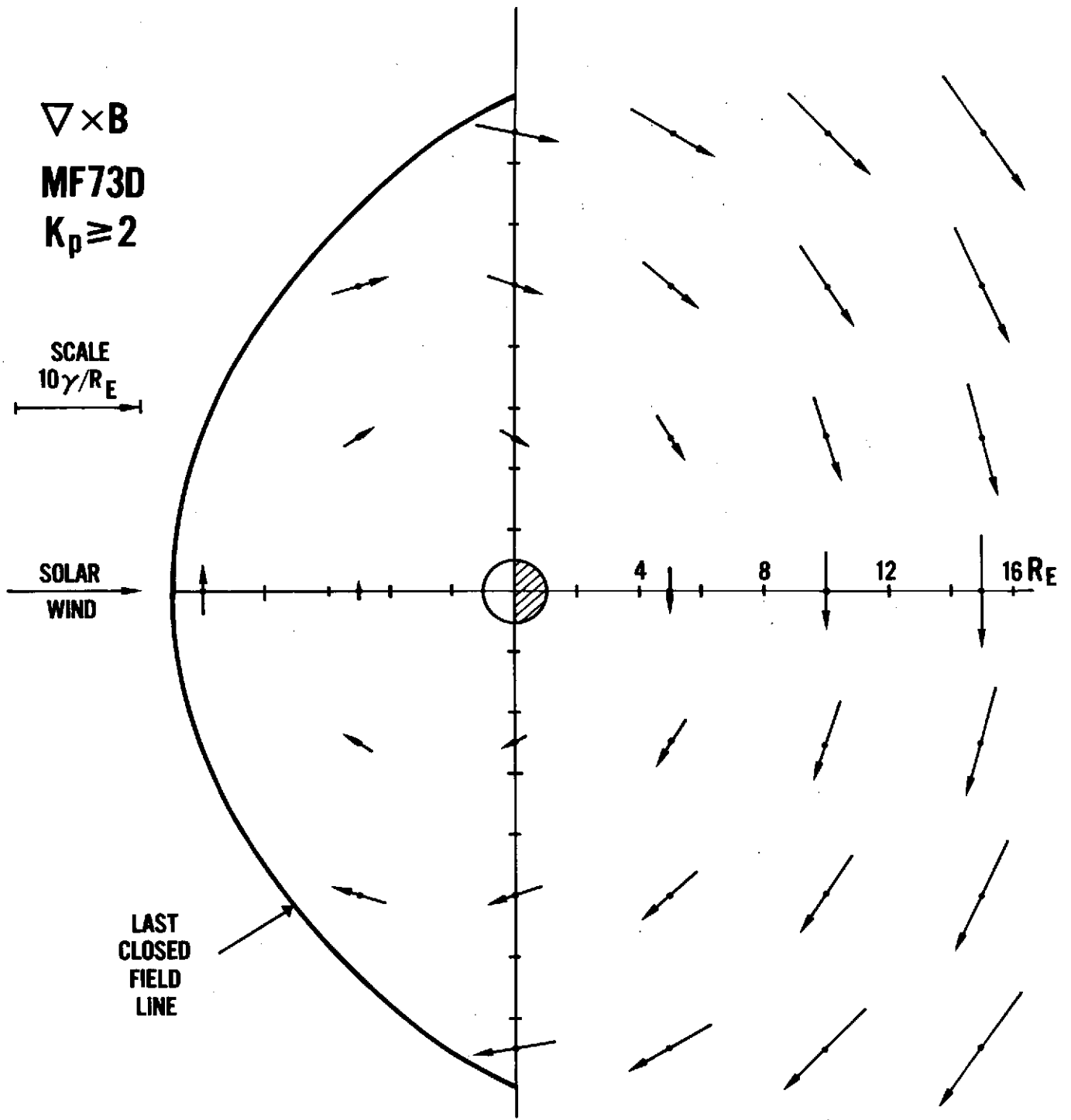Figure 5

Figure 6

Figure 7

Figure 8

LAST CLOSED FIELD LINES

Figure 9

Figure 10

Figure 11